AJR FOCUS ON:

Prostate MRI and 3D MR Spectroscopy: How We Do It

Sadhna Verma[1]
Arumugam Rajesh[2]
Jurgen J. Fütterer[3]
Baris Turkbey[4]
Tom W. J. Scheenen[3]
Yuxi Pang[4]
Peter L. Choyke[4]
John Kurhanewicz[5]

Keywords: choline, citrate, metabolites, MRI, MR spectroscopy, oncologic imaging, polyamines, prostate cancer, prostate

DOI:10.2214/AJR.10.4312

Received January 20, 2010; accepted without revision January 22, 2010.

A. Rajesh was named the 2010 Lee F. Rogers International Fellow by the American Roentgen Ray Society.

[1]Department of Radiology, University of Cincinnati Medical Center, 234 Goodman St., PO Box 670761, Cincinnati, OH 45267-0761. Address correspondence to S. Verma.

[2]Department of Radiology, University Hospitals of Leicester, NHS Trust Leicester General Hospital, Leicester, United Kingdom.

[3]Department of Radiology, Radboud University, Nijmegen Medical Centre, Nijmegen, The Netherlands.

[4]Molecular Imaging Program, National Cancer Institute, National Institutes of Health, Bethesda, MD.

[5]Departments of Radiology, Urology, and Pharmaceutical Chemistry, Prostate Imaging Group, and Biomedical NMR Laboratory, University of California, San Francisco, San Francisco, CA.

CME
This article is available for CME credit.
See www.arrs.org for more information.

AJR 2010; 194:1414–1426

0361–803X/10/1946–1414

OBJECTIVE. This review is a primer on the technical aspects of performing a high-quality MRI and MR spectroscopic imaging examination of the prostate.

CONCLUSION. MRI and MR spectroscopic imaging are useful tools in the localization, staging, and functional assessment of prostate cancer. Performing a high-quality MR spectroscopic examination requires understanding of the technical aspects and limitations of spectral acquisition, postprocessing techniques, and spectral evaluation.

MR spectroscopic imaging (MRSI) is emerging as a useful technique for evaluating the extent and aggressiveness of primary and recurrent prostate cancer. This technique differs from other MRI techniques in that abnormalities of tissue metabolism rather than anatomy are assessed. Interest in MRSI has been driven by the need to map the functional characteristics of tumors to more specifically determine their location. MRI and MRSI both are used for detailed anatomic and metabolic evaluation of the prostate. The purpose of this review is to provide a primer and step-by-step guide to performing a high-quality MRI/MRSI examination and to describe the technical aspects of spectral acquisition, postprocessing techniques, and spectral evaluation.

MRI

The common clinical magnetic field strengths for MRI of the prostate are 1.5 T and 3 T. The combined use of endorectal and pelvic phased-array coils is recommended to maximize the signal-to-noise ratio [1]. For endorectal coil placement, the patient assumes the left lateral decubitus position, a digital rectal examination is performed, and the endorectal balloon with the coil inside (Prostate eCoil, Medrad) (Fig. 1) is inserted and inflated with 60 cm^3 or more of air or 40–60 mL of liquid, such as perfluorocarbon, barium sulfate, or another fluid with tissue-matching susceptibility. Use of an inert liquid instead of air can greatly reduce susceptibility differences between the endorectal balloon and the prostate. This reduction in susceptibility differences around the prostate facilitates magnetic field homogenization in the prostate, dramatically improving the quality of spectral data from the prostate. The pelvic phased-array coil is placed on the patient, who is in the supine position for acquisition of MR images from the prostate to the aortic bifurcation.

Adequate endorectal coil placement is crucial to acquiring optimal spectra. Therefore, it is important to check the scout images at the start of the examination (Fig. 2) to make sure that the sensitive volume of the coil is centered on the prostate in the sagittal plane and that there is not a large tilt (≤ 20°) of the probe in relation to the prostate in the axial plane. To avoid hemorrhage-related artifacts due to previous biopsy, a delay of at least 8 weeks is recommended between the MRI examination and the last biopsy [2]. Hemorrhage interferes with all sequences used to image the prostate, including the MRSI sequences. In cases in which the study is urgent, a quick axial T1-weighted sequence can be performed before placement of the endorectal coil to ensure that a diagnostic-quality study will be possible.

Three manufacturers of MRI systems have prostate spectroscopy packages for 1.5-T and 3-T systems (Table 1). Although imaging parameters depend on the type of imaging unit used and the field strength, we discuss the general principles. Specific information on each vendor is shown in Table 1. At a minimum, the following imaging sequences are recommended: axial T1-weighted sequence

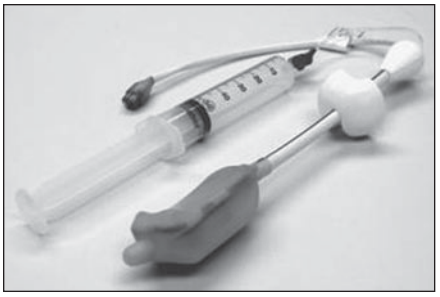

Fig. 1—Photograph shows expandable endorectal coil.

for detection of nodal disease and postbiopsy hemorrhage in the prostate and high-resolution small field-of-view (FOV) T2-weighted images in at least two planes for local assessment of prostate cancer and to localize the volume for prostate spectroscopy. The rest of this review focuses on the acquisition, processing, and interpretation of MRSI data.

MRSI

MRSI of the prostate is typically performed with a combination of point-resolved spectroscopy (PRESS) volume localization and 3D chemical shift imaging (CSI) [3] rather than the traditional single-voxel or 2D MRSI technique used for many years for brain imaging. The setup is a bit more complicated, and there are several critical steps in the process of prescribing the correct volume.

In selecting the PRESS volume, it is important to include the entire prostate while simultaneously minimizing coil interfaces (particularly adjacent to the rectum) and contamination from the seminal vesicles and fat adjacent to the prostate [4–7]. It is also critical to carefully identify areas of fat, because lipid signals can significantly distort the spectra across a large part of the FOV. Contamination of spectra with lipid signals over multiple voxels can be decreased by filtering [8]. Very selective saturation bands are used to further minimize the lipid signals [9]. The spectroscopic imaging box is prescribed on the high-resolution axial T2-weighted images, and the metabolic information is then superimposed on the corresponding T2-weighted anatomic images [5].

Spectroscopic Imaging Parameters

Specific imaging parameters vary by vendor. Parameters are chosen to obtain 3D chemical shift images from as much of the prostate as possible. Although most malignant tumors occur in the posterior aspect of the prostate, a large number of malignant tumors missed at ultrasound-guided biopsy occur in the anterior and lateral aspects, and it is important to have adequate spectral coverage of these areas. Three-dimensional CSI requires phase encoding in three dimensions, conventionally known as frequency, phase, and slice. Acquisition time and coverage of the prostate are the main considerations in choosing the matrix dimensions. Although it is not absolutely necessary, the most common approach in selecting the FOV and the spacing parameters is to prescribe isotropic CSI voxels. The in-plane CSI voxel size is determined by the FOV divided by the corresponding direction in the phase-encoding matrix. Depending on the vendor, these matrix dimensions can be chosen either freely or as a power of 2.

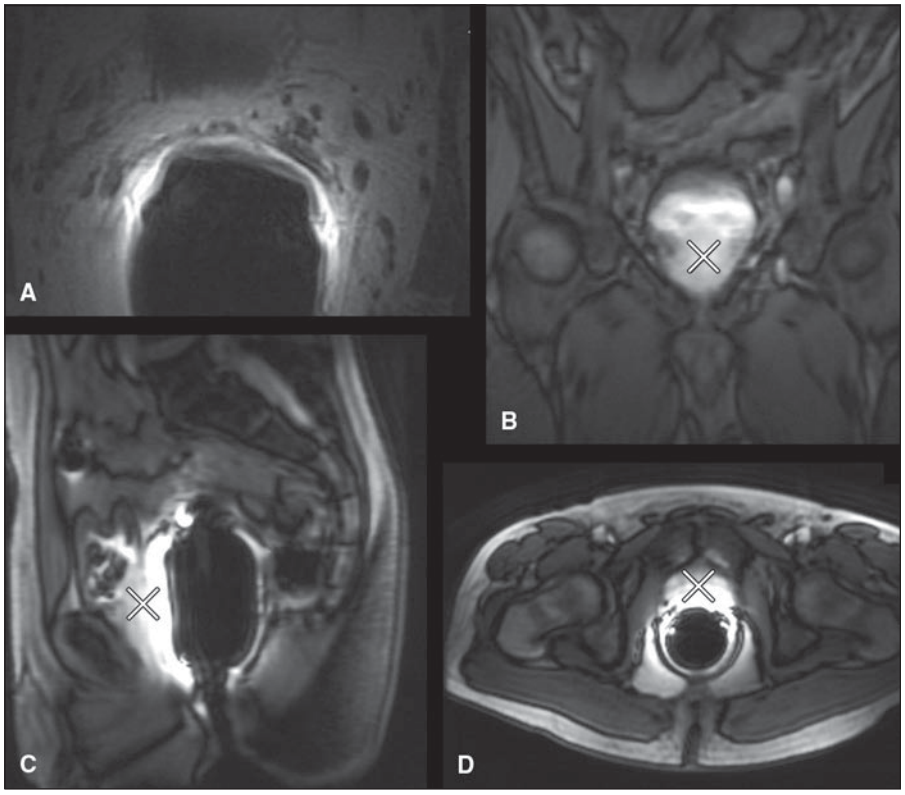

Fig. 2—62-year-old man with prostate cancer.
A–D, MR images show steps in evaluation of coil position. For optimal coil placement, coil chosen should cover entire prostate (X) (**A** and **B**). Signal coverage should be checked from superior to inferior aspect with sagittal fast spin-echo localizer images (**C**). Anterior to posterior coverage (**D**) should be checked to make sure coil is not rotated.

The key differences in the spectroscopy protocols of the 1.5-T and 3-T systems include modifications of the PRESS sequence typically used for spectral acquisition and changes in the TE used [8, 10, 11]. These changes are mandated by the changes in the spectral shape of the strongly coupled citrate spin system at 3 T relative to 1.5 T [12]. The pulse sequence and acquisition parameters therefore must be reoptimized to obtain completely upright citrate resonance. One 3-T spectral acquisition approach (Malcolm Levitt composite-pulse decoupling sequence [MLEV]-PRESS) operates with trains of 180° pulses during TE to refocus the citrate resonance, resulting in a completely upright citrate resonance at a sufficiently short TE (85 milliseconds) [10]. Conventional PRESS has multiple possibilities for an in-phase spectral shape of citrate [13]. Prostate MRSI at 3 T also can provide twofold higher spatial resolution over 1.5 T, but the result can be longer acquisition times to cover the entire gland with conventional phase encoding [14].

PRESS CSI acquisition times can be further lengthened if longer TR is used to reduce partial saturation effects. One solution is having full flexibility in choosing matrix dimensions in a weighted phase-encoding acquisition scheme [8, 11]. Another option is incorporation of echo-planar readout trajectories in one dimension of the pulse sequence [14]. This method reduces the minimum MRSI acquisition time eightfold, providing ample possibilities for additional

TABLE 1: Imaging Parameters for Prostate Spectroscopy Packages of Three Manufacturers

Parameter	GE Healthcare	Philips Healthcare	Siemens Healthcare
Patient position	Supine	Supine	Supine
Patient entry	Feet first	Head first	Feet first
Coil	Endorectal and 8-channel phased-array coil	Endorectal and 16-channel surface coils	Endorectal
Plane	Oblique	Oblique axial	Axial
Code	MR spectroscopy	NA	MR spectroscopy
Pulse sequence	Prose	3D point-resolved spectroscopy	Point-resolved spectroscopy
Gradient mode	Whole (NA)	NA	Whole (NA)
Imaging options	Extended dynamic range, spectral-spatial radiofrequency	NA	Weighted elliptic sampling
Acquisition timing			
No. of echoes	1	1	1
TE (ms)			
1.5 T	130	130	120
3 T	85	100	145
TR (ms)			
1.5 T	1,000	1,000	650
3 T	1,300	980	750
Flip angle	90°–180°–180°	90°–180°–180°	90°–180°–180°
Echo-train length	NA	NA	NA
Acquisition range			
Field of view (mm)	110	72	Various (e.g., 72 × 72 × 60)
Voxel thickness (mm)	50	60	6
Spacing (mm)	6.9 (first selection)	6.0	6
No. of locations per slab	8	10	10
Acquisition timing			
No. of phase-encoding steps (*x, y, z*)	8	10 × 10 × 10	12
No. of signals acquired	1	1	3–5 weighted averages
Phase field of view	1	72 × 72 × 60 mm^3	NA
Frequency direction	Right to left	Right to left	NA
Automatic center frequency	Water	Water	Water
Autoshim	On	On	On, manual
Phase correction	NA	None	NA

Note—NA = not applicable.

averaging and matrix enlargement at a small cost of sampling efficiency. The short acquisition time with this method reduces the 3-T prostate MRI/MRSI examination time and allows longer TR and acquisition of large spectral arrays covering the entire prostate at high spatial resolution of 0.154 cm^3 [14].

Prescribing Spectroscopy Volume (Rectangular PRESS Box) and Saturation Bands

The robust acquisition of prostate MRSI data requires accurate volume selection with either optimized 180° pulses or spectral–spatial pulses for refocusing the signals [15, 16] and efficient outer volume suppression [17]. This technique involves placement of the spectroscopy volume of interest (VOI) and outer volume saturation bands. In prescribing the VOI, also known as the spectroscopy PRESS box, it is preferred that the VOI be placed and sized on axial or axial oblique images that correspond to the small-FOV T2-weighted images. It is important to clearly identify the top slice in which the prostate is present without the seminal vesicles and the bottom slice where the apex of the gland is visible (Fig. 3). The in-plane rectangular spectroscopy box is adjusted to maximize inclusion of the entire prostate and minimize extraprostatic tissue. The box should extend from the rectal wall to the most anterior aspect of the prostate and fit the gland as closely as possible (Fig. 4). The prostate capsule, which appears as a thin black rim around the prostate, can be used as a guide. The in-plane MRSI voxel size will be determined with the FOV and the selected phase-encoding matrix. An increase in the phase-encoding matrix to obtain higher spatial resolution for a

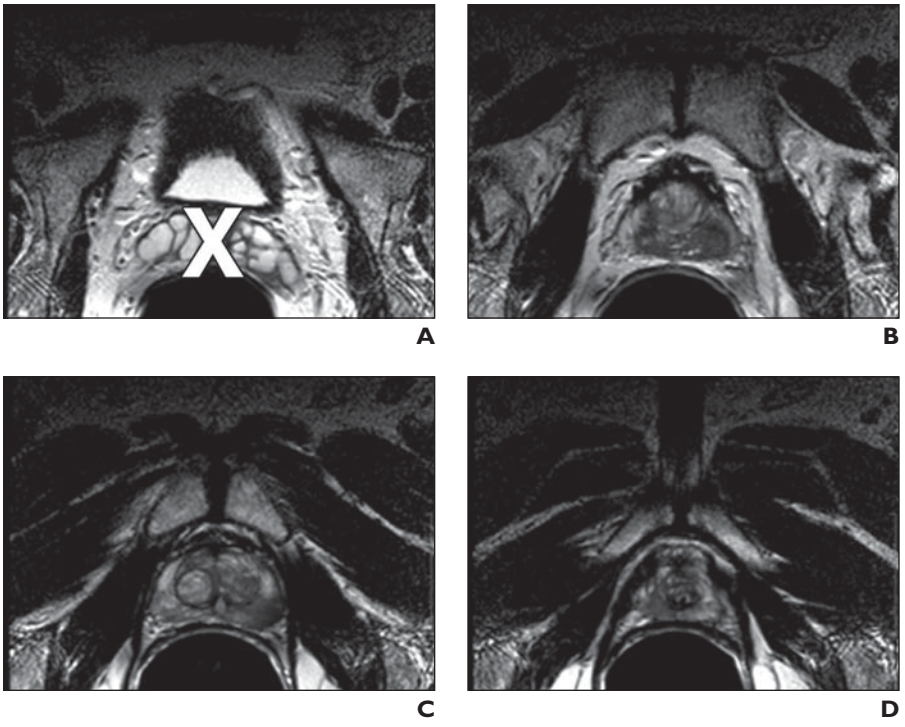

Fig. 3—70-year-old man with prostate cancer. **A–D,** MR images show goals in volume prescription are to cover whole gland, especially peripheral zone, without seminal vesicles; minimize inclusion of air interface; and minimize lipid inclusion. Image **A** was obtained at level of seminal vesicle (X). Images **B**–**D** are regions to be included in volume prescription: **B**, level of prostate base; **C**, level of midgland; and **D**, level of prostate apex.

given FOV will result in a dramatic increase in the spectral acquisition time if conventional phase encoding is used.

An axial MRI slice obtained at mid gland encompassing the largest cross section of the prostate is selected, and outer volume saturation bands (20–30 mm thick) are placed around the box at oblique angles. The saturation band thickness and positioning are adjustable. The saturation bands are used to shape the VOI box to better match the prostate shape and eliminate unwanted extraprostatic tissue by cutting off the edges of the rectangular box (Fig. 5A). This step is taken to partially counteract the inclusion of any fat in the MRSI volume itself and to reduce the possibility of lipid contamination from the surrounding tissue (Fig. 5B). Positioning of the superior and inferior saturation bands often is performed with high-resolution sagittal images of the prostate. These bands are placed almost to the top and bottom of the spectroscopy voxel but not overlapping the edge because the overlap can cause excessive suppression of the spectral signal in the last CSI slice. One saturation band is placed to saturate the border with the rectum. It is placed parallel to the coil and the posterior edge of the spectroscopy voxel to suppress artifacts from the rectal wall interfaces and the thin layer of tissue between the prostate and the rectum. Once all saturation bands are placed, all images are checked for correct positioning of both the spectroscopy box and saturation bands.

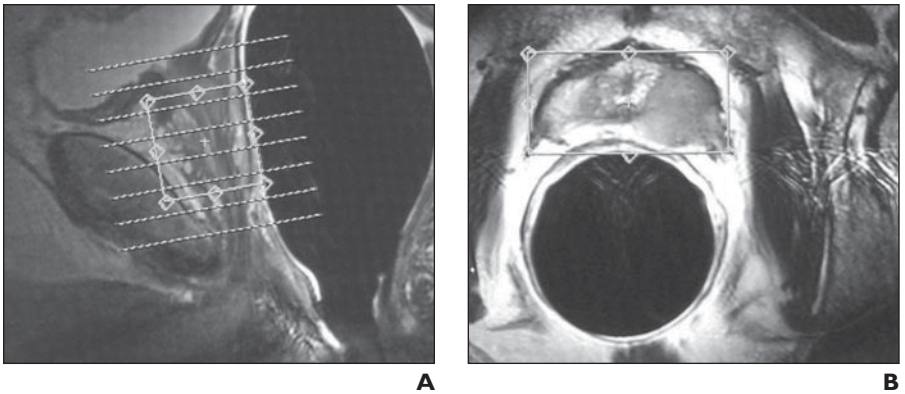

Fig. 4—50-year-old man with biopsy-proven prostate cancer of Gleason grade 7 (4 + 3). **A** and **B,** Axial (**A**) and axial oblique (**B**) MR images show prescription of volume of interest. Volume box should be placed and sized on image.

Shimming (Improving B_0 Homogeneity)

Critical to the acquisition of good-quality prostate spectra is optimization of the B_0 homogeneity of the PRESS-selected VOI. This process typically involves use of a combination of the standard automatic shim provided by the manufacturer and, if necessary, manual touching up of the *x, y,* and *z* gradients. During manual shimming, the technologist or spectroscopist uses both the magnitude and shape of the free-induction decay and Fourier-transformed water resonance to assess the quality of the shim. Slight improvements in the shim can make a huge difference in the quality of the spectra. Specifically, good B_0 homogeneity is necessary for sufficient water and lipid suppression. Water and lipid suppression is achieved by generation of either frequency-selective Mescher and Garwood (MEGA) and band-selective inversion with gradient dephasing (BASING) pulses within the PRESS volume selection [18, 19] or spectral–spatial pulses capable of both volume selection and frequency selection [15, 16]. During the spectral acquisition, the spectra can be observed in the display windows to determine whether large lipid resonance obscures the prostate metabolite resonance peak. This problem can be corrected by checking the placement of the saturation bands to eliminate the lipid signals. Broad metabolite peaks are indicative of poor homogeneity. If the peaks are too broad, the VOI or saturation bands should be rechecked and repositioned, and manual shimming should be performed. Manual adjustments should be made in a minimum of three primary *x, y,* and *z* gradients (Fig. 6). If a system has the capability, higher-order shimming would be expected to further improve the results. The full width at half maximum line width of residual water peak, reported as LnWdth, is a good indicator of spectral homogeneity. The line width value typically increases as the VOI increases.

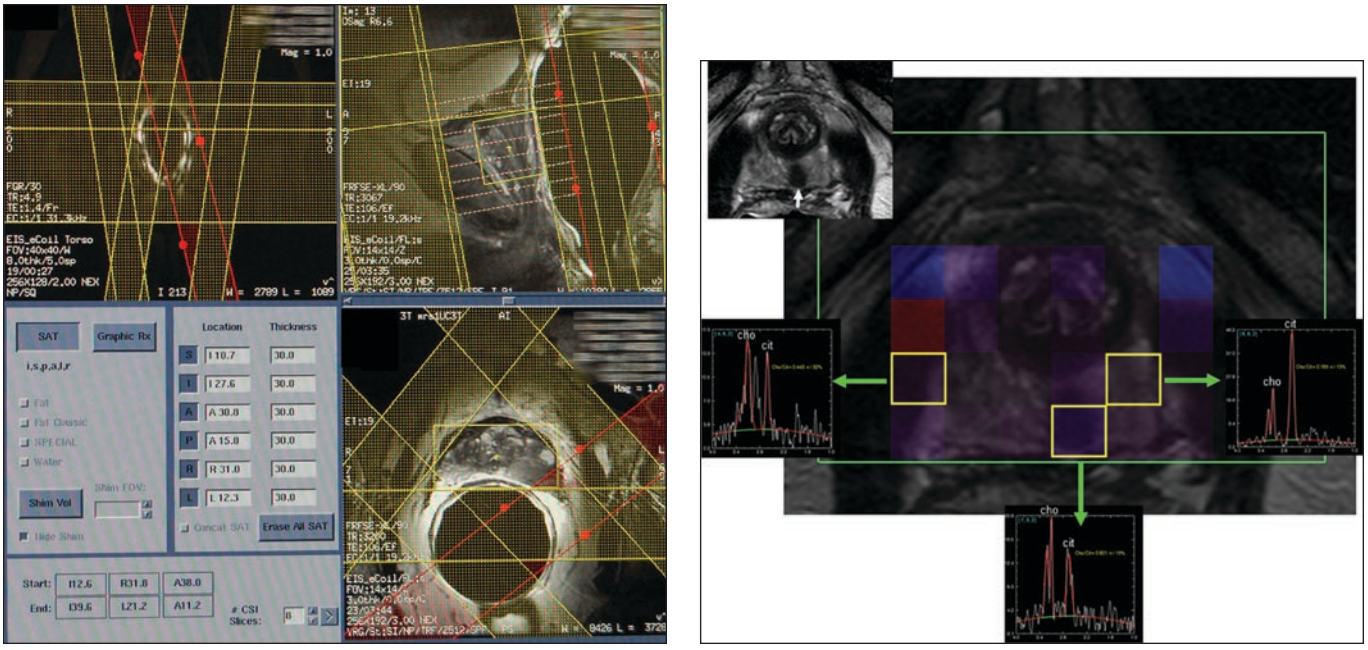

Fig. 5—Saturation band placement.
A, 60-year-old man with prostate cancer and prostate-specific antigen level of 9.2 ng/dL. Axial T2-weighted localizer MR images show prescription of four very selective suppression radiofrequency bands. Two bands are prescribed on sagittal localizer images.
B, 56-year-old man with prostate cancer with serum prostate-specific antigen of 3.3 ng/dL. Pitfall due to low apical periprostatic fat. MR spectroscopic image shows single abnormal voxel with elevated choline to citrate (cho/cit) ratio (0.801) in apical midline peripheral zone. Voxel in left low apical peripheral zone is normal. Voxel on right has elevated cho/cit ratio (0.443) but does not include tumor; elevated cho/cit ratio is secondary to periprostatic fat contamination, which is common pitfall at low apex.

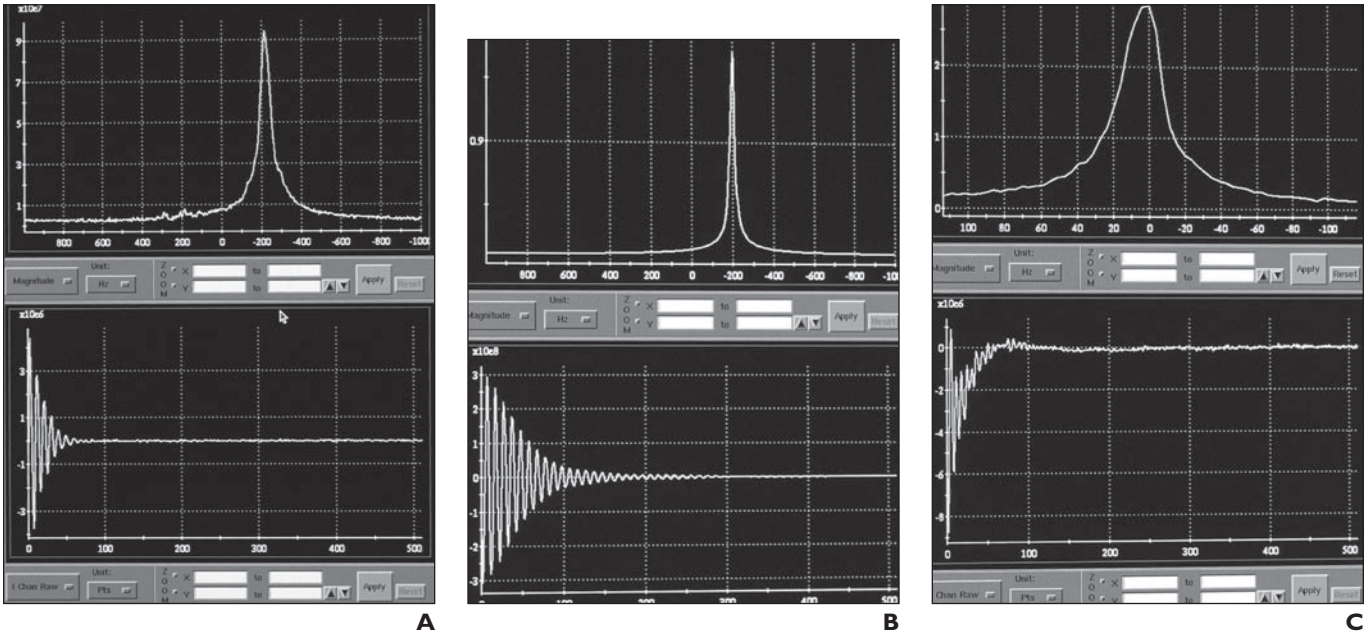

Fig. 6—56-year-old man with biopsy-proven prostate cancer. In shimming of spectroscopy window before acquisition, there are typically several display options for evaluating spectra. In this instance, two display windows are used. Fourier transformation takes time domain function (free-induction decay [*bottom*]) and converts it into frequency domain function (spectrum [*top*]).
A, Example of standard automatic shim spectrum result from entire prostate volume. Top screen shows water peak at –200-Hz off resonance. Shoulder on water peak indicates need for further manual shimming to improve magnetic field homogeneity. It is possible to improve homogeneity through prostate volume by manually adjusting *x, y,* and *z* gradient currents.
B, Optimized gradient shimming. Improving homogeneity through volume of interest by manual adjustment of *x, y,* and *z* gradient currents. With time domain function, it is ideal that decay be as long as possible without evidence of harmonics on display. Goal is to achieve smooth exponential slope of envelope as long in time as possible.
C, Recentering water peak exactly on center frequency. Magnitude display is expanded for very precise recentering of water peak.

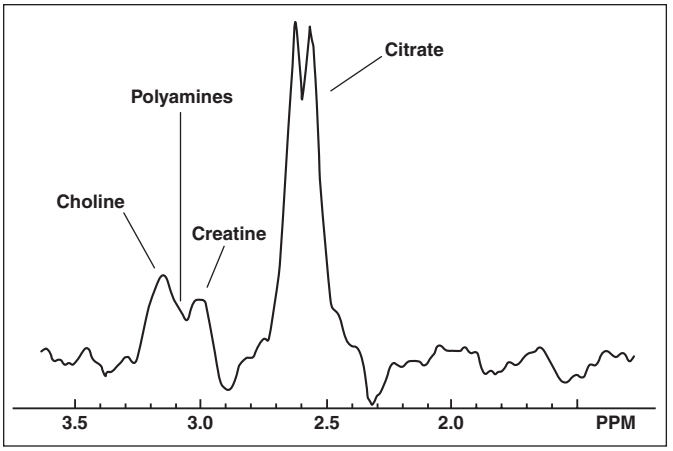

Fig. 7—MR spectra of normal human prostate.

Metabolite Peaks

In MRSI, the metabolites are identified by their resonance frequency (Fig. 7), which is based on the chemical environment of hydrogen atoms. Each chemically nonequivalent proton of a metabolite resonates at a different frequency, often referred to as the chemical shift, which is measured in parts per million (ppm) with reference to water (which is not shifted and has a spectral location of 0 ppm on GE Healthcare MRI systems). However, this setting can vary by MRI vendor. On Siemens Healthcare units, water is set as an anchor at 4.7 ppm. One can choose to shift the center of the spectral bandwidth away from water, for example, to 2.9 ppm, exactly between choline and citrate. It is important to remember that in displaying peak shifts in parts per million rather than Hertz, the designated location for a given metabolite stays the same regardless of the field strength of the system. Thus spectra from a 1.5-T system have the same peak locations as 3-T spectra.

Several key metabolic resonances are identifiable. Principal among these is citrate, a metabolite found in relatively high concentration in the glandular tissue of a healthy prostate [20]. The normal MRI spectrum of the prostate reveals a prominent citrate peak, which often appears as a doublet if the shim is good enough. Spectra with a high signal-to-noise ratio show that the citrate peak has two additional satellite peaks, which have a very small magnitude compared with the center two peaks and are not detected at most clinical MRSI examinations [21]. Depending on the pulse sequence timing, these satellites can have more or less intensity [22]; at 3 T they are an obvious part of the spectral shape of citrate, centered at 2.6 ppm [13].

Other resonances of interest are those of creatine and choline. Choline is a composite peak made up of phospholipid membrane components; the choline level is elevated in many malignant tumors that affect humans, including prostate cancer [23, 24]. Creatine and choline resonate at 3.0 and 3.2 ppm, respectively. Healthy prostate epithelial cells also contain high concentrations of polyamines, particularly spermine. Like the citrate level, polyamine levels are dramatically reduced in prostate cancer [24]. The polyamine peaks lie between the choline and creatine peaks, and because they compose a very broad peak, these resonances usually overlap those of both choline and creatine (Fig. 8A). If present in or too near a voxel, lipid resonance will be well to the right of citrate and typically form a broad hump in the spectrum, rendering it difficult to interpret (Fig. 8B).

Postprocessing

Once acquisition is complete, several correction steps have to be manually or auto-

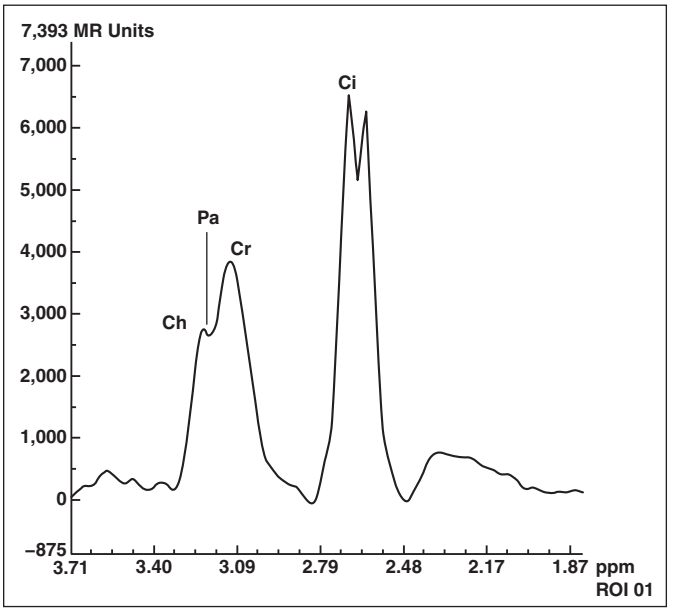

A

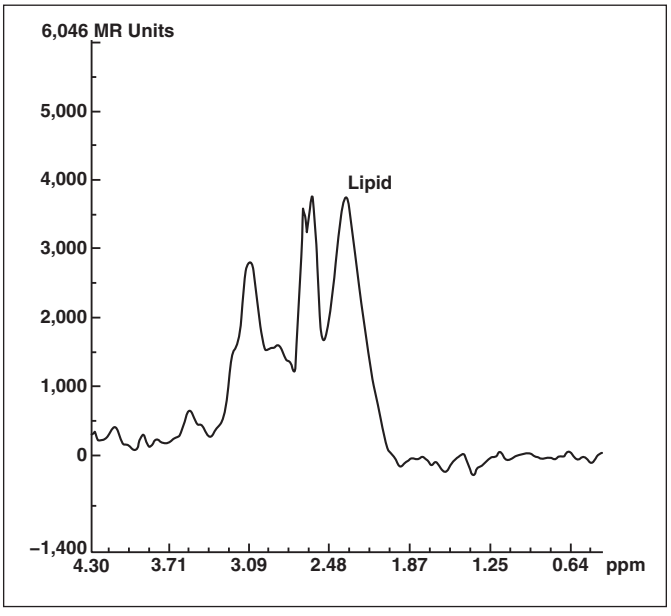

B

Fig. 8—Metabolite peaks in patients with prostate cancer.
A, 62-year-old man with prostate cancer of Gleason grade 7 (3 + 4). Ch = choline, Pa = polyamine, Cr = creatine, Ci = citrate.
B, 65-year-old man with prostate cancer. Spectra show unwanted lipid signal. Large lipid resonance can obscure prostate metabolite resonance peaks.

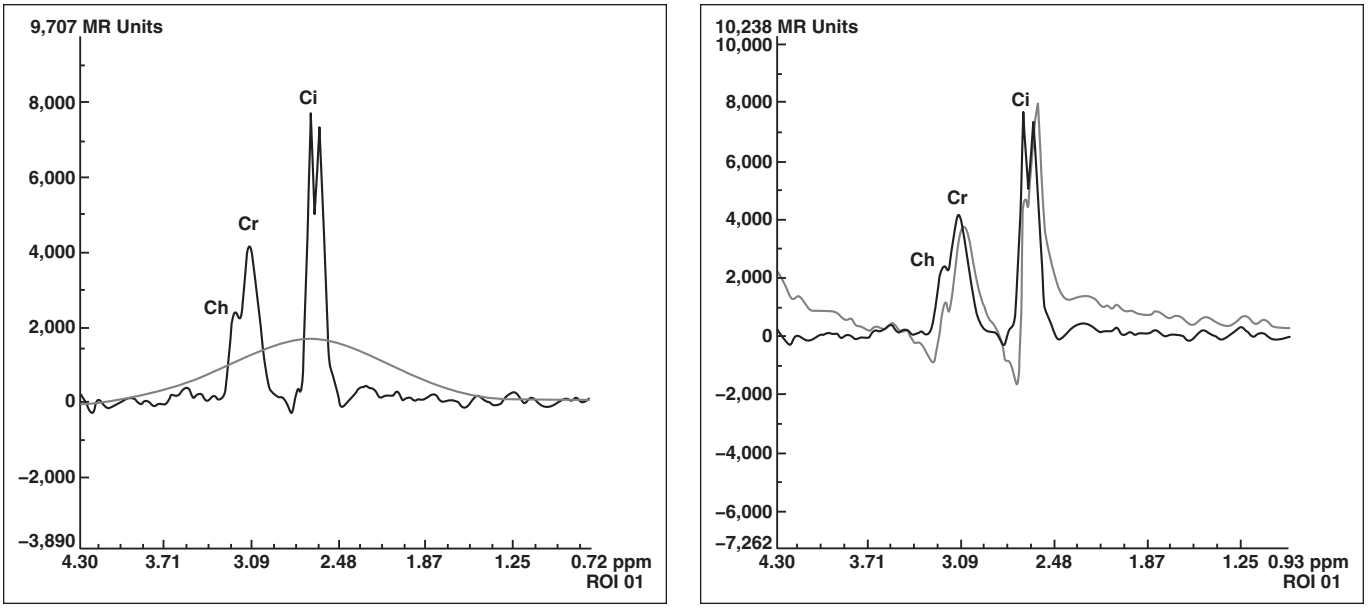

Fig. 9—Adjustments to spectra.
A, Automated baseline correction: sinusoidal curvature of baseline.
B, Automated phase correction.

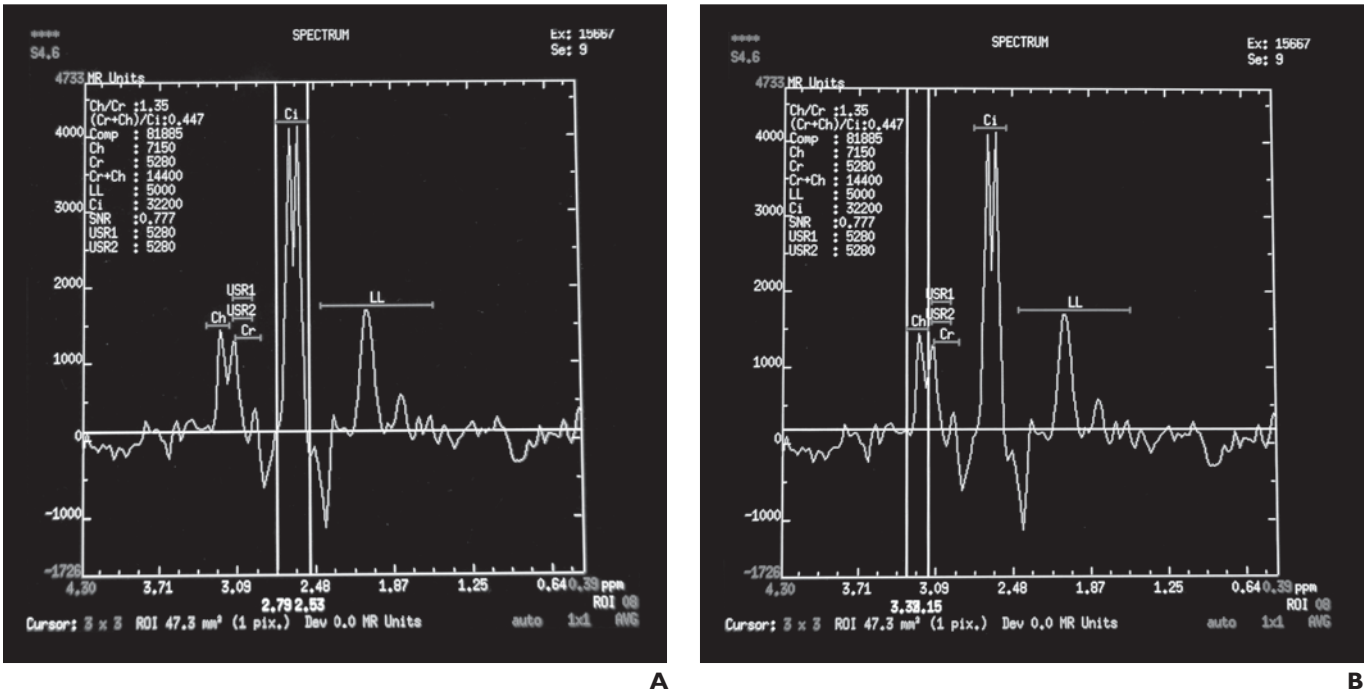

Fig. 10—Set ranges for metabolites.
A, Citrate (Ci) peak
B, Choline (Ch) peak.

matically applied to the spectroscopy data. Historically, MRSI data were taken from the MRI system and processed with in-house research software. In the current commercial MRI/MRSI packages, the MRSI data can be processed and displayed on the MRI unit. The software interfaces differ by manufacturer, but the basic concepts are similar.

For MRSI data, the first processing steps are to combine signals from different coil elements (if more than one are used), construct arrays of spectra by applying time domain apodization and Fourier transformation, and reconstruct the spatial dependence of the data. If weighted acquisition has been used, filtering is applied in the spatial directions before Fourier transformation [8]. The spectral data are transferred from the MRI unit to the workstation

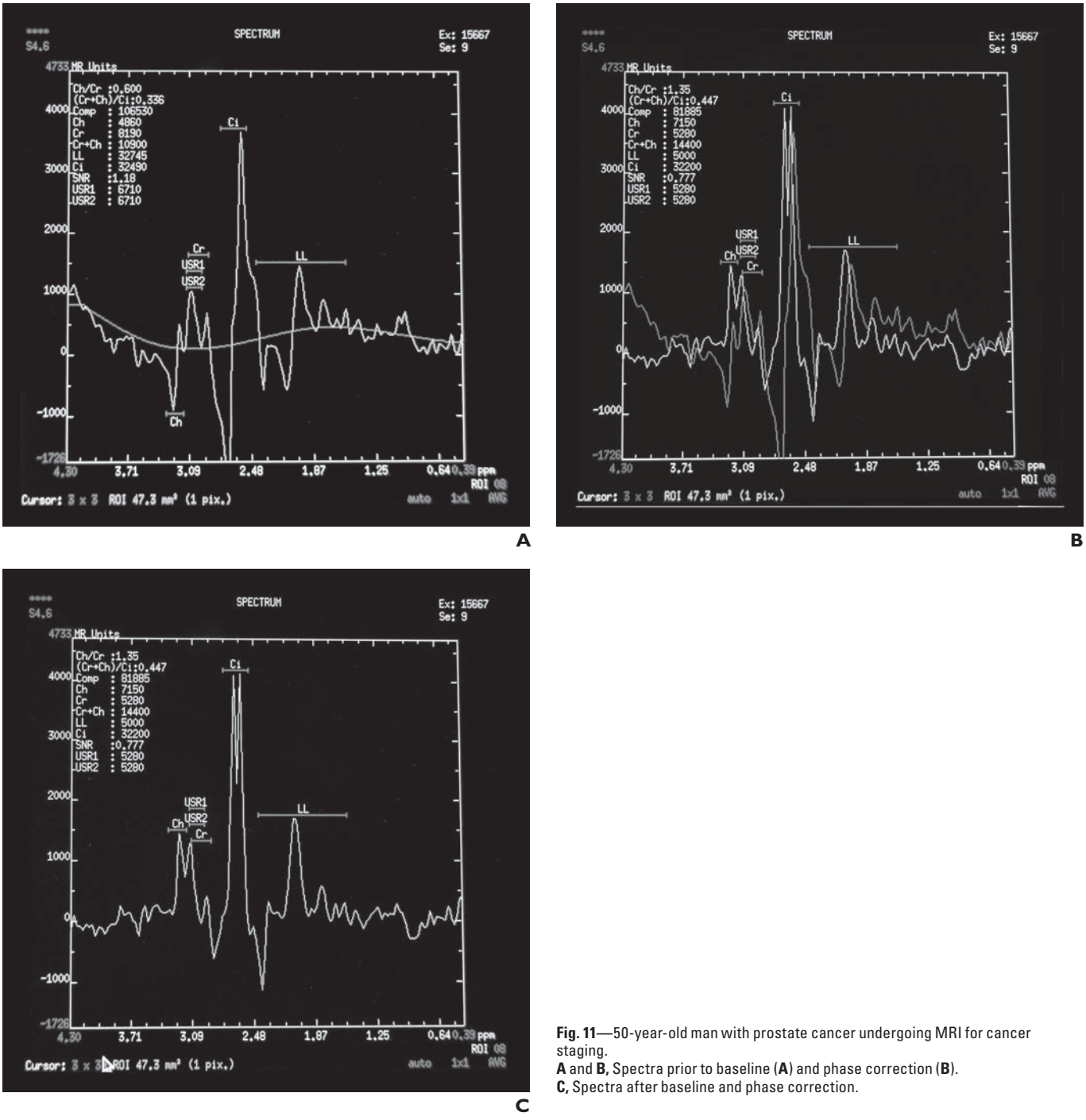

Fig. 11—50-year-old man with prostate cancer undergoing MRI for cancer staging.
A and **B,** Spectra prior to baseline (**A**) and phase correction (**B**).
C, Spectra after baseline and phase correction.

with the corresponding anatomic images, usually high-resolution T2-weighted axial images, into the vendor-specific software program. The MRS images should be surveyed for assessment of overall spectral quality and identification of any particular problem regions. If adequate spectra are obtained, a few adjustments are necessary. The spectroscopy analysis package performs an automatic analysis of the areas under the metabolic peaks, applying a fit to the spectra and providing comparative values of choline, creatine, and citrate and the ratios of these metabolites (Fig. 9).

Baseline and Phase Correction and Calculation of Metabolite Peak Areas

Metabolite ratios are based on the calculated areas under the spectral peaks. For accurate estimation of these areas, it is necessary to correct for constant and spatially dependent frequency and phase shifts and for baseline variations due to broad resonances or residual water. Frequency and phase corrections can be achieved with a water reference or by use of the spectra themselves to estimate correction parameters. Baseline corrections and estimation of peak parameters are best achieved

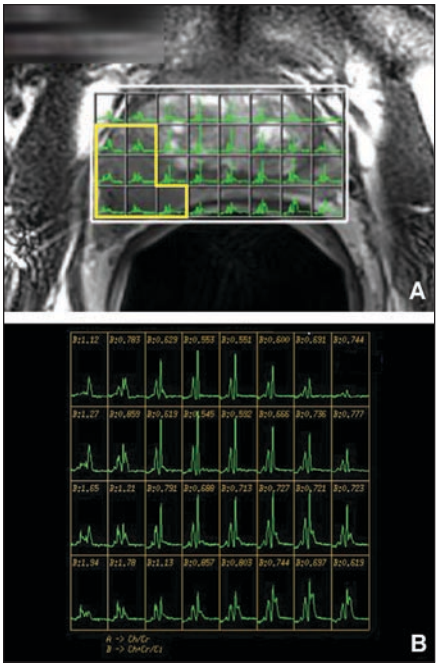

Fig. 12—62-year-old man with biopsy-proven prostate cancer with prostate-specific antigen level of 6.8 ng/dL and Gleason grade 6 (3 + 3).
A, T2-weighted axial MR image shows 1.7-cm low-signal-intensity mass in right mid gland with prostate capsular bulge.
B, Spectroscopy grid from **A** shows abnormal ratio of choline and creatine to citrate ratio corresponding to low-signal-intensity mass.

by use of prior knowledge of the approximate relative position of the major peaks in the spectrum (Fig. 10). The software normally provides an initial estimate of the appropriate spectral baseline and phase corrections and allows users to subsequently manually adjust baseline and phase shifts. Peak areas can be estimated by integration of a range of frequencies or by fitting baseline subtracted data as a sum of components with particular line shapes [25, 26] (Fig. 11). Whichever fitting algorithm is used, the number of spectra involved makes it critical that the procedure be fully automated and that it be robust to low signal-to-noise ratios and missing peaks.

MRSI produces arrays of spectra from contiguous voxels that are approximately 0.15–1.0 cm^3 in volume and cover most or all of the prostate. Because MRSI and MRI are performed in the same examination, the data sets are already in alignment and can be directly overlaid. In this way, areas of anatomic abnormality (decreased signal intensity on T2-weighted images) can be correlated with the corresponding area of metabolic abnormality (increased choline and decreased citrate and polyamine levels).

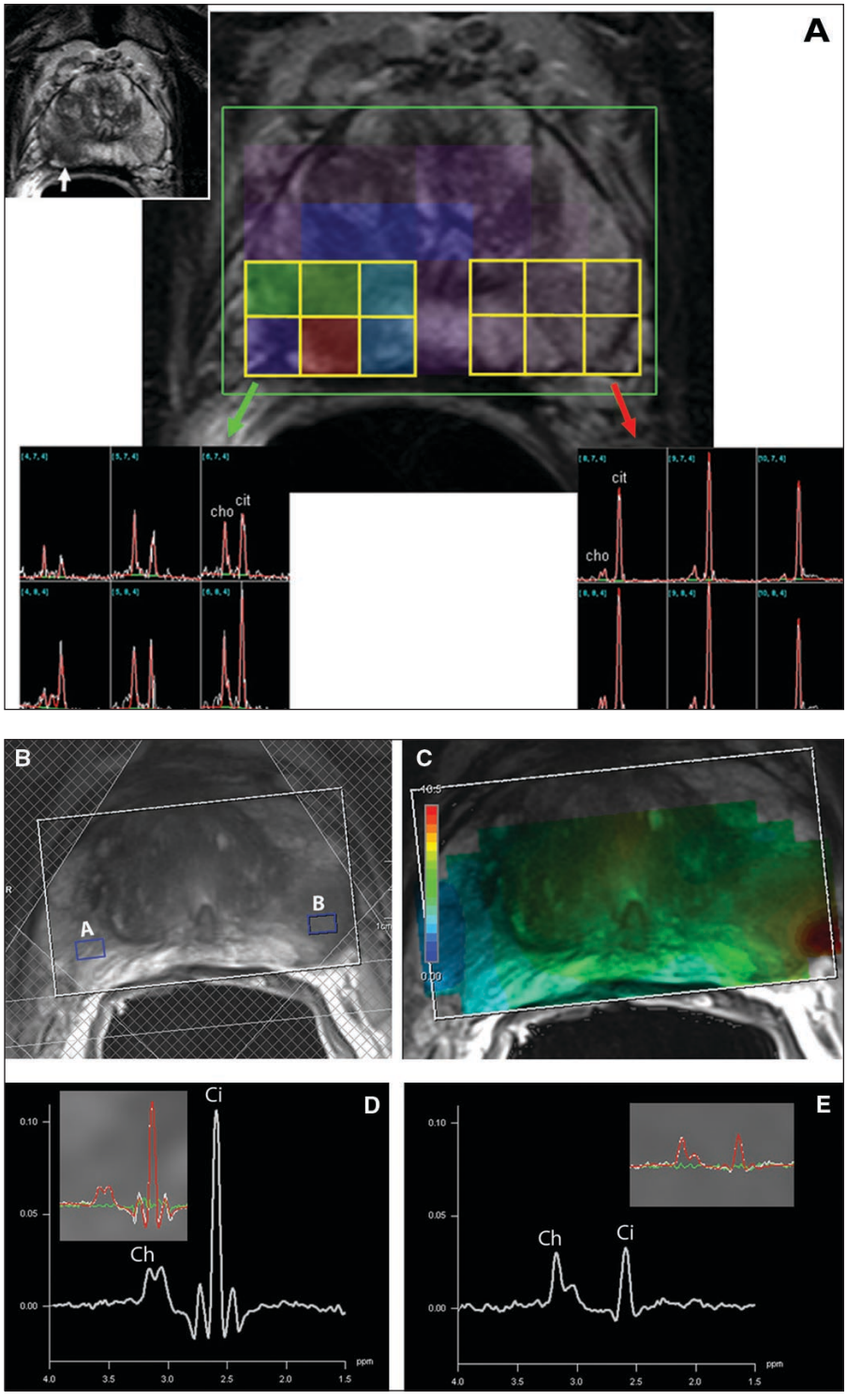

Fig. 13—Examples of output seen by radiologist.
A, 73-year-old man with prostate cancer with serum prostate-specific antigen level of 45 ng/dL. MR spectroscopic images corresponding to voxels axial T2-weighted MR image show increased choline (cho) to citrate (cit) ratio (*green arrow*) in right mid peripheral zone tumor (*white arrow*). Red arrow indicates normal cho/cit ratio in left mid peripheral zone.
B–E, 58-year-old man with prostate cancer. Axial 3-T T2-weighted MR images (**B** and **C**) show tumor in left peripheral zone. Spectra (**D** and **E**) corresponding to partitions (A and B) of MRI image show healthy peripheral zone tissue and tumor. Insets in spectra are automated fits to spectra that quantify signals from choline, creatine, and citrate. These signals can be combined in map of ratio of choline and creatine to citrate.

Several approaches have been used to display the combination of anatomic and metabolic information derived from simultaneous MRI and MRSI. These include superimposing a grid on the MR image and plotting the corresponding arrays of spectra (Fig. 12) and calculating images of the spatial distribution of metabolites to be placed as overlays on the corresponding MR images. In clinical use, the spectral data and corresponding T2-weighted images are sent to a PACS as screen-save images or as new DICOM images (Fig. 13) for interpretation by the radiologist.

Spectral Evaluation

Interpretation of prostate spectra requires both knowledge of what constitutes a clinically interpretable spectrum and an understanding of the underlying biochemical processes and morphologic changes that result in metabolic changes. Prostate MRSI spectra are considered clinically interpretable if they are not contaminated by insufficiently suppressed water or lipid and have resolvable metabolite peaks with peak area-to-noise ratios greater than 5 to 1. Interpretation of prostate spectra requires knowledge of the complex zonal anatomy of the gland, which can have differing metabolic profiles due to the presence of differing tissue types [27]. Of particular importance to the interpretation of prostate spectra is the amount of glandular versus stromal tissue present in the voxel, which differs substantially by zone of the prostate. High levels of citrate and intermediate levels of choline have been observed throughout the normal peripheral zone. Consistent with the reduction in glandular cell content of the central prostate (central zone and transition zones), a marked decrease in citrate in this region relative to the normal peripheral zone has been observed [27]. Nonglandular elements of the prostate include the anterior fibromuscular band and periurethral tissues, and these regions have threefold lower citrate levels [27]. In addition, in tissue surrounding the ejaculatory ducts, urethra, and seminal vesicles, the in vivo choline peak can be elevated owing to the presence of high levels of glycerophosphocholine in the fluid in these structures (Fig. 14).

The first steps in analysis of spectral data are to identify whether the spectral voxels originate from the peripheral zone or the central gland and to determine whether the voxels are contaminated by glycerophosphocholine from fluid in the ejaculatory ducts, urethra, and seminal vesicles (Fig. 15). Because at least 68% of malignant tumors of the prostate and the most clinically significant tumors originate in the peripheral zone, MRI/MRSI research has focused on peripheral zone cancer. Having found metabolic changes in choline, polyamine, and citrate levels in regions of prostate cancer, Jung et al. [28] devised a standardized scoring system for the spectral evaluation of peripheral zone spectral data, and the combined cen-

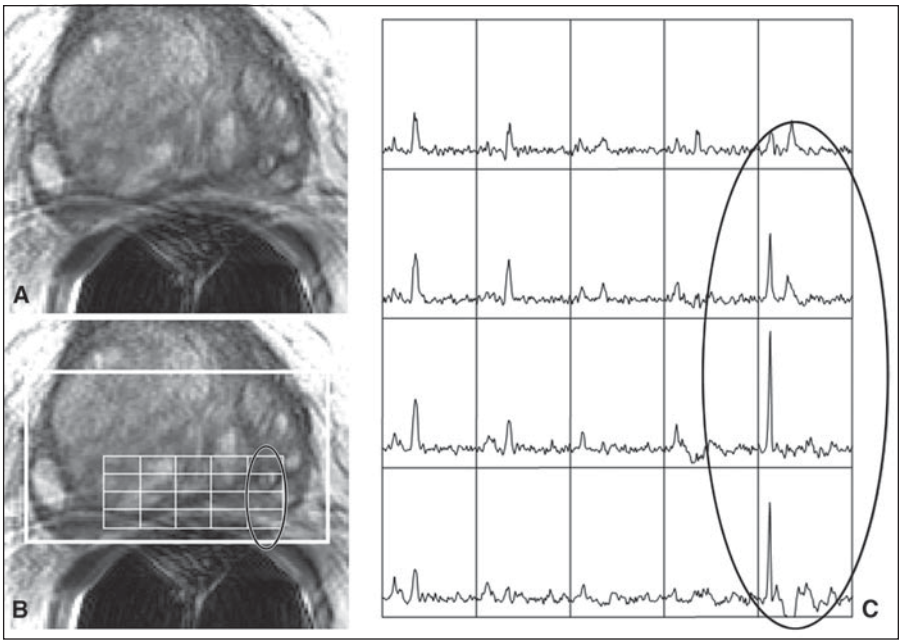

Fig. 14—56-year-old man with biopsy-proven prostate cancer.
A and **B,** T2-weighted axial MR images at level of base of prostate (**A**) and corresponding image (**B**) with overlaid point-resolved spectroscopy volume (*bold white outline*) and spectral grid. Oval outline indicates seminal vesicles bleeding into left lateral aspect.
C, Spectra (*oval*) corresponding to oval in **B** show very high resonance resembling choline peak due to very high glycerophosphocholine level in seminal fluid. This finding is often misinterpreted as prostate cancer.

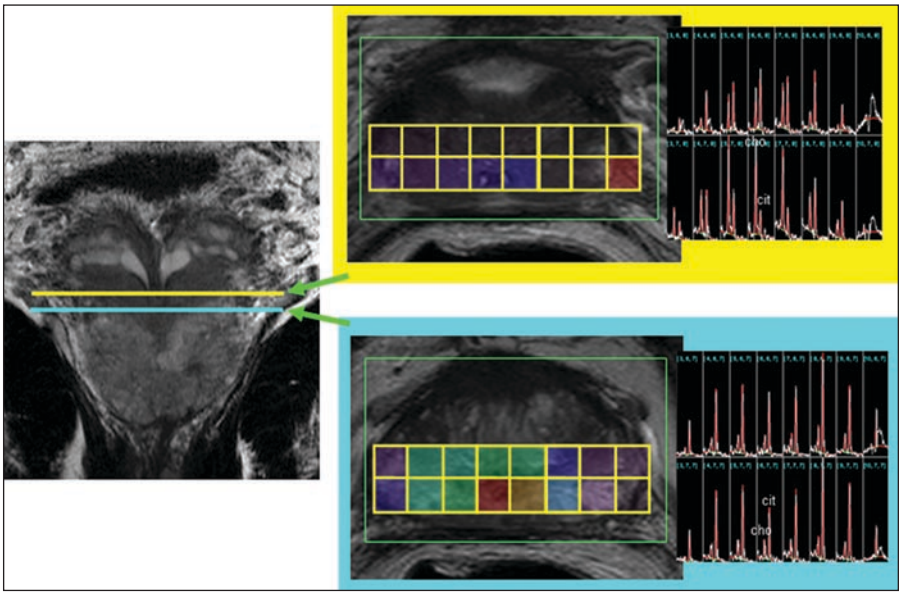

Fig. 15—57-year-old man with prostate cancer with serum prostate-specific antigen level of 4.5 ng/dL. Pitfall due to seminal vesicle contamination. MR spectroscopic image shows increased choline-to-citrate ratios in voxels at base due to seminal vesicle contamination (*yellow*). MR spectroscopic image in more inferior location (*turquoise*) shows normal choline-to-citrate ratios.

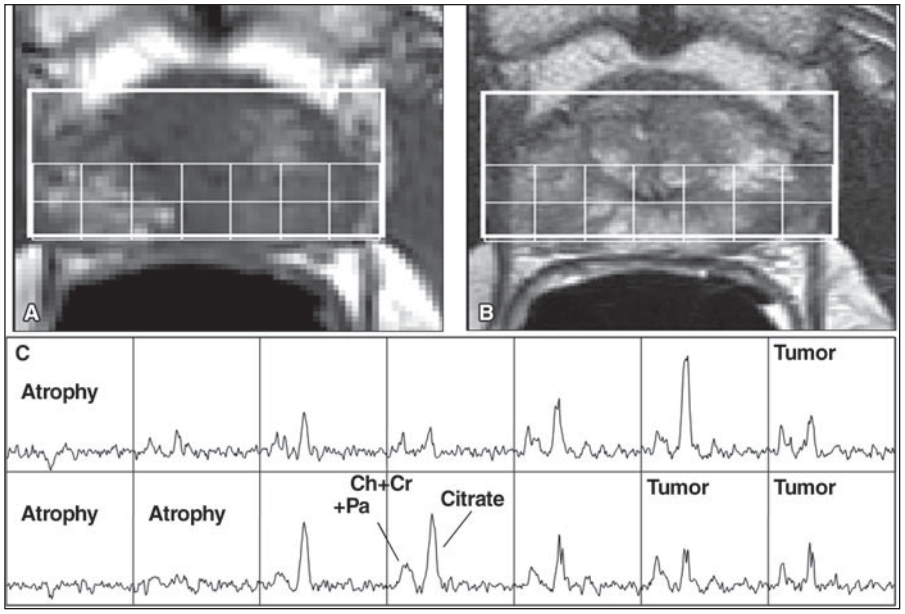

Fig. 16—64-year-old man with prostate cancer with prostate-specific antigen level of 7.2 ng/dL and Gleason grade of 6 (3 + 3).
A, Axial T1-weighted MR image shows extensive postbiopsy hemorrhage (high signal intensity) on left lobe of prostate 3 weeks after biopsy.
B, Axial T2-weighted image corresponding to **A** shows low signal intensity in same region.
C, Spectral array shows loss of spectral signal in region of postbiopsy hemorrhage. Patients have had both metabolic atrophy and changes in metabolite levels in regions of extensive hemorrhage soon after biopsy, confounding ability to metabolically detect prostate cancer. Ch = choline, Cr = creatine, Pa = polyamines.

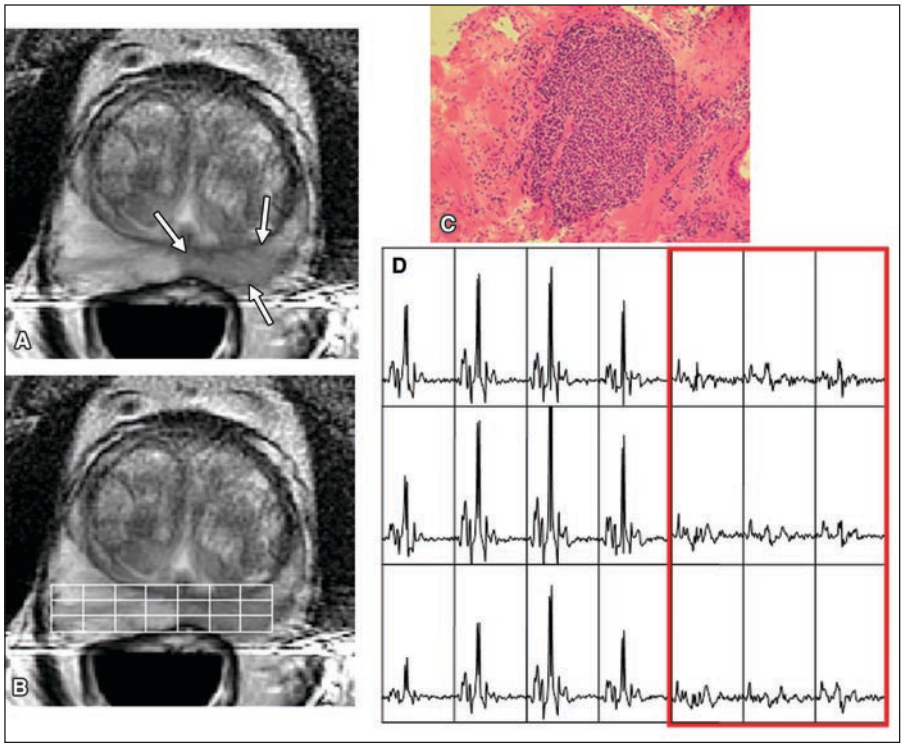

Fig. 17—61-year-old man with elevated prostate-specific antigen level of 4.0 ng/dL.
A and **B,** Axial T2-weighted image (**A**) at mid gland level of prostate and corresponding image with overlaid spectral grid (**B**) show region of decreased signal intensity (*arrows,* **A**) in left lobe consistent with prostate cancer.
C, Histopathologic image shows extensive acute inflammation in left lobe of prostate. Biopsy findings were negative for cancer.
D, Spectral array corresponding to **A** and **B** shows reduction in overall spectral signal but elevated choline to citrate ratio in region of T2 abnormality, also suggesting prostate cancer.

tral gland data were added later [29]. The result is a final score from 1 to 5 designed so that the following interpretative scale can be applied: 1, probably benign; 2, possibly benign; 3, equivocal; 4, possibly malignant; 5, probably malignant. In addition to using the 5-point scoring system, readers interpreting the images can designate spectra as unusable if marked lipid contamination or misalignment of metabolite resonance peaks is present. The 5-point scale has been found reasonably accurate and to have excellent interobserver agreement ($\kappa = 0.80$) in differentiation of benign from malignant tissue [28].

In general, peripheral zone voxels in which the ratio of choline and creatine to citrate is at least 2 SDs greater than the average ratio are considered to represent possible cancer. Voxels are considered highly suggestive of cancer if the ratio of choline and creatine to citrate is more than 3 SDs greater than the average ratio [28]. The exact ratio can vary with equipment and setting, so no fixed threshold ratios are reported. Ratios at 3 T also differ slightly from those at 1.5 T because of differences in the shape of the citrate spectrum [30]. In addition, because the choline-to-citrate ratio is the major parameter derived from MRSI, it is crucial that the quality of the spectra be evaluated before the

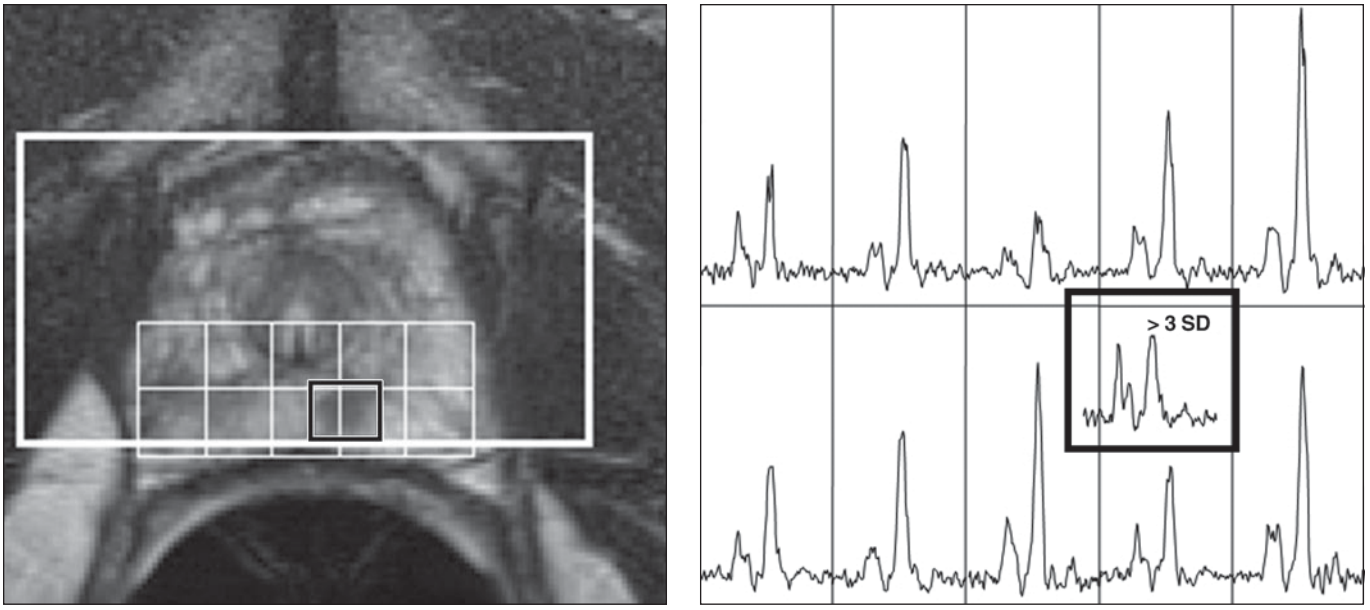

Fig. 18—54-year-old man with prostate cancer.
A, Axial T2-weighted MR image at level of apex of prostate with overlaid point-resolved spectroscopy box (*bold white line*) and spectral grid.
B, Spectral array corresponding to **A** shows small region of low signal intensity in left apex corresponds to region of biopsy-proven prostate cancer. Region of low T2 signal intensity is split between two voxels (> 3 SD) in original spectral array. Because volume MRI and MR spectroscopic imaging data are collected, spectroscopic voxels can be shifted in postprocessing to optimally encompass region of abnormality on MR image.

numerical ratios are read. A simple reading of the ratios can be misleading if the ratios are based on artifact-riddled spectra with a noisy baseline.

Other confounding factors in interpretation of prostate spectral data include postbiopsy changes, coexisting confounding benign pathologic changes (prostatitis, benign prostatic hyperplasia [BPH]), and the mix of cancerous and healthy tissue in small-volume (< 0.5 cm^2) early-stage tumors [31]. The timing of MRI/MRSI after transrectal biopsy is critical because of biopsy-induced spectral changes. It has been found [2] that spectral degradation is inversely related to time from biopsy ($p < 0.01$). In that study, the mean percentage of degraded peripheral zone voxels was 18.5% within 8 weeks of biopsy compared with 7% after 8 weeks, an argument for delaying MRSI for at least 8 weeks after biopsy (Fig. 16).

Results [32, 33] have suggested that in at least some cases the MRI/MRSI appearance of acute prostatitis can mimic that of cancer (Fig. 17). Malignant tumors of the central gland (transition zone and central zone) also have proved particularly difficult to discriminate with MRI/MRSI [34]. There is considerable overlap of low signal intensity on T2-weighted images and metabolism on MRS images in regions of central gland tumor with predominately stromal BPH [34]. Regions of predominately glandular BPH have markedly elevated levels of citrate and polyamines because they are secretory products of healthy and hyperplastic glandular tissues. In predominately stromal tissues, however, such as predominately stromal BPH, citrate and polyamine levels are very low, similar to those observed in cancer. As in cancer, the choline level can be somewhat elevated because increased cellular proliferation occurs in BPH, as it does in cancer.

Although prostatitis and stromal BPH are the most common benign confounding factors in the misdiagnosis of prostate cancer with MRI/MRSI, prostate cancer also can be missed when signal originating from surrounding benign tissues masks the metabolic fingerprint of cancer, particularly in cases of small infiltrative lesions. Specifically, benign glandular tissues have very high signal intensity on T2-weighted MR images and very high levels of polyamines and citrate, and these signals dominate the prostate spectrum. It is possible to use a procedure referred to as voxel shifting to reduce partial volume effects by optimally aligning the spectral voxel with small tumors during postprocessing (Fig. 18). Predominately mucinogenic prostate cancer is also difficult to detect with MRI/MRSI [35]. On T2-weighted MR images, these tumors have high signal intensity due to the presence of the pockets of mucin. At MRSI, the spectral signal intensity is often very low owing to the low density of prostate cancer cells [35].

Conclusion

MRSI of the prostate can be a useful diagnostic tool for detecting prostate cancer. Establishing and running a successful MRSI protocol involves more attention to detail and technical knowledge than do most MRI sequences. MRSI is an evolving functional tool in the assessment of prostate cancer, and this review should help readers understand the critical steps involved in performing a high-quality MRSI examination.

References

1. Heijmink SW, Futterer JJ, Hambrock T, et al. Prostate cancer: body-array versus endorectal coil MR imaging at 3 T—comparison of image quality, localization, and staging performance. *Radiology* 2007; 244:184–195
2. Qayyum A, Coakley FV, Lu Y, et al. Organ-confined prostate cancer: effect of prior transrectal biopsy on endorectal MRI and MR spectroscopic imaging. *AJR* 2004; 183:1079–1083

3. Brown TR, Kincaid BM, Ugurbil K. NMR chemical shift imaging in three dimensions. *Proc Natl Acad Sci USA* 1982; 79:3523–3526
4. Claus FG, Hricak H, Hattery RR. Pretreatment evaluation of prostate cancer: role of MR imaging and ^{1}H MR spectroscopy. *RadioGraphics* 2004; 24[suppl 1]:S167–S180
5. Coakley FV, Kurhanewicz J, Lu Y, et al. Prostate cancer tumor volume: measurement with endorectal MR and MR spectroscopic imaging. *Radiology* 2002; 223:91–97
6. Hricak H. MR imaging and MR spectroscopic imaging in the pre-treatment evaluation of prostate cancer. *Br J Radiol* 2005; 78(spec no 2):S103–S111
7. Kurhanewicz J, Vigneron DB, Hricak H, Narayan P, Carroll P, Nelson SJ. Three-dimensional H-1 MR spectroscopic imaging of the in situ human prostate with high (0.24-0.7-cm3) spatial resolution. *Radiology* 1996; 198:795–805
8. Scheenen TW, Klomp DW, Roll SA, Fütterer JJ, Barentsz JO, Heerschap A. Fast acquisition-weighted three-dimensional proton MR spectroscopic imaging of the human prostate. *Magn Reson Med* 2004; 52:80–88
9. Tran TK, Vigneron DB, Sailasuta N, et al. Very selective suppression pulses for clinical MRSI studies of brain and prostate cancer. *Magn Reson Med* 2000; 43:23–33
10. Cunningham CH, Vigneron DB, Marjanska M, et al. Sequence design for magnetic resonance spectroscopic imaging of prostate cancer at 3 T. *Magn Reson Med* 2005; 53:1033–1039
11. Fütterer JJ, Scheenen TW, Huisman HJ, et al. Initial experience of 3 tesla endorectal coil magnetic resonance imaging and ^{1}H-spectroscopic imaging of the prostate. *Invest Radiol* 2004; 39:671–680
12. Mulkern RV, Bowers JL. Calculating spectral modulations of AB systems during PRESS acquisitions. *Magn Reson Med* 1993; 30:518
13. Scheenen TW, Gambarota G, Weiland E, et al. Optimal timing for in vivo ^{1}H-MR spectroscopic imaging of the human prostate at 3T. *Magn Reson Med* 2005; 53:1268–1274
14. Chen AP, Cunningham CH, Ozturk-Isik E, et al. High-speed 3T MR spectroscopic imaging of prostate with flyback echo-planar encoding. *J Magn Reson Imaging* 2007; 25:1288–1292
15. Cunningham CH, Vigneron DB, Chen AP, et al. Design of symmetric-sweep spectral-spatial RF pulses for spectral editing. *Magn Reson Med* 2004; 52:147–153
16. Schricker AA, Pauly JM, Kurhanewicz J, Swanson MG, Vigneron DB. Dualband spectral-spatial RF pulses for prostate MR spectroscopic imaging. *Magn Reson Med* 2001; 46:1079–1087
17. Tran TKC, Vigneron DB, Sailasuta N, et al. Very selective suppression pulses for clinical MRSI studies of brain and prostate cancer. *J Magn Reson Imaging* 2000; 43:23–33.
18. Mescher M, Merkle H, Kirsch J, Garwood M, Gruetter R. Simultaneous in vivo spectral editing and water suppression. *NMR Biomed* 1998; 11:266–272
19. Star-Lack J, Nelson SJ, Kurhanewicz J, Huang LR, Vigneron DB. Improved water and lipid suppression for 3D PRESS CSI using RF band selective inversion with gradient dephasing (BASING). *Magn Reson Med* 1997; 38:311–321
20. Costello LC, Franklin RB. Concepts of citrate production and secretion by prostate. Part 1. Metabolic relationships. *Prostate* 1991; 18:25–46
21. Mulkern RV, Bowers JL, Peled S, Kraft RA, Williamson DS. Citrate signal enhancement with a homonuclear J-refocusing modification to double-echo PRESS sequences. *Magn Reson Med* 1996; 36:775–780
22. van der Graaf M, Jager GJ, Heerschap A. Removal of the outer lines of the citrate multiplet in proton magnetic resonance spectra of the prostatic gland by accurate timing of a point-resolved spectroscopy pulse sequence. *MAGMA* 1997; 5:65–69
23. Heerschap A, Jager GJ, van der Graaf M, et al. In vivo proton MR spectroscopy reveals altered metabolite content in malignant prostate tissue. *Anticancer Res* 1997; 17:1455–1460
24. Kurhanewicz J, Swanson MG, Nelson SJ, Vigneron DB. Combined magnetic resonance imaging and spectroscopic imaging approach to molecular imaging of prostate cancer. *J Magn Reson Imaging* 2002; 16:451–463
25. Derby K, Hawryszko C, Tropp J. Baseline deconvolution, phase correction, and signal quantification in Fourier localized spectroscopic imaging. *Magn Reson Med* 1989; 12:235–240
26. Spielman D, Webb P, Macovski A. Water referencing for spectroscopic imaging. *Magn Reson Med* 1989; 12:38–49
27. Coakley FV, Kurhanewicz J, Qayyum A. Prostate. In: Edelman RR, Hesselink JR, Zlatkin MB, Crues JV, eds. *Clinical magnetic resonance imaging.* Philadelphia, PA: Elsevier, 2006:2906–2931
28. Jung JA, Coakley FV, Vigneron DB, et al. Prostate depiction at endorectal MR spectroscopic imaging: investigation of a standardized evaluation system. *Radiology* 2004; 233:701–708
29. Fütterer JJ, Scheenen TW, Heijmink SW, et al. Standardized threshold approach using three-dimensional proton magnetic resonance spectroscopic imaging in prostate cancer localization of the entire prostate. *Invest Radiol* 2007; 42:116–122
30. Scheenen TW, Heijmink SW, Roell SA, et al. Three-dimensional proton MR spectroscopy of human prostate at 3 T without endorectal coil: feasibility. *Radiology* 2007; 245:507–516
31. Kurhanewicz J, Vigneron DB. Advances in MR spectroscopy of the prostate. *Magn Reson Imaging Clin N Am* 2008; 16:697–710
32. Engelhard K, Hollenbach HP, Deimling M, Kreckel M, Riedl C. Combination of signal intensity measurements of lesions in the peripheral zone of prostate with MRI and serum PSA level for differentiating benign disease from prostate cancer. *Eur Radiol* 2000; 10:1947–1953
33. van Dorsten FA, van der Graaf M, Engelbrecht MR, et al. Combined quantitative dynamic contrast-enhanced MR imaging and (1)H MR spectroscopic imaging of human prostate cancer. *J Magn Reson Imaging* 2004; 20:279–287
34. Zakian KL, Eberhardt S, Hricak H, et al. Transition zone prostate cancer: metabolic characteristics at ^{1}H MR spectroscopic imaging—initial results. *Radiology* 2003; 229:241–247
35. Westphalen AC, Coakley FV, Kurhanewicz J, Reed G, Wang ZJ, Simko JP. Mucinous adenocarcinoma of the prostate: MRI and MR spectroscopy features. *AJR* 2009; 193:870; [web]W238–W243

FOR YOUR INFORMATION

This article is available for CME credit. See www.arrs.org for more information.